In situ synthesis of CuO nanoparticles over functionalized mesoporous silica and their application in catalytic syntheses of symmetrical diselenides

Trisha Das,[a] Rana Chatterjee,[b] Adinath Majee,[b] Hiroshi Uyama,[c] David Morgan[d] and Mahasweta Nandi*[a]

[a]*Integrated Science Education and Research Centre, Siksha Bhavana, Visva-Bharati University, Santiniketan 731 235, India*

Email: mahasweta.nandi@visva-bharati.ac.in

[b]*Department of Chemistry, Siksha Bhavana, Visva-Bharati University, Santiniketan 731235, India*

[c]*Department of Applied Chemistry, Graduate School of Engineering, Osaka University, 2-1 Yamadaoka, Suita, Osaka, 565-0871, Japan*

[d]*Cardiff Catalysis Institute, School of Chemistry, Cardiff University, Park Place, Cardiff CF10 3AT*

Abstract

A versatile and novel catalyst, CuO nanoparticles immobilized over functionalized mesoporous silica (**nCuO-FMS**), has been synthesized over an organically modified mesoporous silica framework following a facile synthetic route. The surface of the silica support (SBA-15) is first grafted with 3-aminopropyl silane group and then further functionalized with *tris*(4-formylphenyl)amine. The reaction is performed in such a way that few -CHO groups remain free for further functionalization. Finally, the CuO nanoparticles immobilized mesoporous silica is obtained by a one pot reaction between the functionalized silica, 2-aminophenol and $CuCl_2$. The product obtained has been used as a catalyst for the synthesis of symmetrical diselenide in presence of KOH as base and dimethyl sulphoxide (DMSO) as the solvent. The materials have been characterized thoroughly by powder X-ray diffraction, nitrogen adsorption-desorption studies, transmission electron microscopy, thermal analysis, and different spectroscopic techniques. The Cu content of the sample has been determined by atomic absorption spectrophotometric (AAS) analysis. Products of the catalytic studies have been identified and estimated by ^{1}NMR spectroscopy. Almost 78% isolated yield could be achieved at 363 K within 3 hours of the reaction and the catalyst, **nCuO-FMS**, can be recycled at least up to five catalytic cycles.

Keywords: Mesoporous silica, functionalization, CuO nanoparticle, heterogeneous catalyst, Se-Se coupling

Introduction

It is known that metal containing heterogeneous catalysts are advantageous over their homogeneous counterparts due to multiple reasons like recyclability, easy recovery, high surface accessibility and often economic with respect to conventional catalysts which can be used just for one time. However, leaching is a typical problem for heterogeneous catalytic systems and in such cases it becomes difficult to ascertain whether the metal ion bound to the solid support or the metal ion leached into the solution is responsible for catalyzing the reaction. To overcome this problem, the metal ion should strongly interact with the heterogeneous support so that it does not get detached from the solid framework during the liquid phase catalytic process. Different types of solid supports *e.g.* polymers,[1] zeolite,[2] alumina,[3] silica,[4] graphene,[5] mesoporous carbon,[6] carbon nanotubes,[7] metal-organic framework,[8] metal oxide nanoparticles,[9] *etc*.[10-12] have been used for the successful syntheses of heterogeneous catalysts. Among these, mesoporous silica is often chosen as solid supports because of their better interaction with the metal centers and accessibility to the substrates. This takes place due to their large surface area[13] which significantly increases the efficiency of the catalysts. Apart from this, it is also possible to tune the pore size of the mesoporous silica matrix as per the specific requirement. Silicate-based structures are generally robust and thermally and chemically stable. Functionalization of their framework can be done easily to introduce hydrophobicity through insertion of various organic moieties. Moreover, if such organic functionalities are heteronuclear molecules then various heteroatoms like N, O, S can be introduced into the materials taking their advantage. Introduction of such groups can modify affinities of the functionalized silica based materials towards specific substrates as well as tune the overall acid base character of the framework.

Metal centers can interact and get attached to such modified frameworks *via* covalent interaction or hard-soft interaction based on the heteroatoms that can be chosen judiciously to solve the purpose.

Over the last two decades and also at present, a considerable amount of interest has been focused on research based on the use of nanostructured metal based catalysts. Such catalysts have shown their potential utility and played pivotal role in several types of organic syntheses and methodologies. Nanoparticles based metal catalysts exhibit special properties and have distinctive physical, chemical, magnetic and optical properties which are completely different from their bulk counter-parts.[14] This can be attributed to their relatively larger surface area compared to the same mass in bulk form and the Quantum effects that begin to dominate their behavior at the nanoscale. For these qualities, nanoparticles have been in use extensively for applications in the fields of catalysis, electronics and photonics. In the field of organic syntheses, metal oxide nanoparticles based catalysts are known to be very effective and fruitful due to their various advantages of a heterogeneous catalyst.[15-17] They are superior over the conventional metal catalysts because of their greater surface exposure, high reactivity and high thermal resistance thus exhibiting higher product yields with better atom economy. Copper oxide (CuO) nanoparticle is one of these important

classes of materials which have been used as catalysts for the development of a number of organic transformations. The effectiveness of using CuO nanoparticle-based catalyst in the area of organic synthesis is well documented in the literature.[18-23]

Organochalcogen compounds are known to function as biologically active molecules[24,25] and have been used as reaction intermediates and reagents in various organic syntheses.[26-28] Apart from these, the organoseleno compounds have found important applications as antioxidant, anti-ulcer and anti-inflammatory agents.[29-31] Several organoseleno compounds have been used as therapeutic agents in the treatment of cancer and various infectious diseases and as apoptosis inducers.[32-33] These compounds also play a vital role in the fields of materials science and nanotechnology.[34,35] For such immense contribution of the organoseleno compounds (especially the diselenides) across several fields of application, there is considerable demand for the preparation of these compounds both in academia and industry. Accordingly, several methods have been developed for the syntheses of diselenide compounds.[36-43] Among these, a method developed by Braga *et.al* is particularly interesting where diselenide compounds have been synthesized using powder CuO nanoparticle as catalyst.[44] In line with this, we have tried to design a mesoporous silica based heterogeneous catalyst containing immobilized CuO nanoparticles instead of the commercially available CuO nanoparticle powder to perform catalytic reactions leading to the formation of diselenides. We have prepared CuO nanoparticles immobilized over functionalized mesoporous silica (**nCuO-FMS**) through a one-pot synthetic strategy (Scheme 1). CuO nanoparticles are spontaneously formed *in situ* under the reaction conditions in presence of the *tris*(4-formyl phenyl)amine grafted mesoporous silica, 2-aminophenol and $CuCl_2$. **nCuO-FMS** has been used as a catalyst for the cost effective syntheses of diselenide compounds, including diaryl diselenides. It could be established that the presence of a catalytic amount of this CuO nanoparticle-based catalyst immensely influence the progress of the reaction, where as in absence of the catalyst the reaction does not proceed. To the best of our knowledge, this is the first report of a CuO nanoparticle based heterogeneous catalyst for the syntheses of diselenides using a neat, facile and innovative technique.

Experimental Details

Materials and physical measurements

All the chemicals used in the syntheses have been obtained from commercial sources and used without further purification. FT-IR spectra of the samples have been collected on a Spectrum Two, Perkin Elmer spectrometer using attenuated total reflectance (ATR) method. Thermogravimetric analyses (TGA) have been performed under N_2 atmosphere (flow rate: 50 cc/min) from room temperature to 1073 K (at heating rate of 2 K/min) using a Perkin Elmer STA-6000 thermal analyzer. Low and high angle powder X-ray diffraction patterns of the samples have been collected on a Bruker D-8 Advance diffractometer using Ni-

filtered Cu- $K\alpha$ radiation (λ = 1.5406 Å) at 40 kV and 40 mA). N_2 sorption isotherms of the samples are measured using a NOVA 2200e Surface Area and Pore Size Analyzer, Quantachrome Instruments, USA at 77 K. Before performing the measurements, the samples are degassed for 8-12 h at 353, 393 or 423 K depending on the nature of the samples and the specific surface areas are obtained using Brunauer-Emmett-Teller (BET) method. For obtaining the pore size distributions, non-local density functional theory (NLDFT) model has been used. The transmission electron microscopic (TEM) images have been recorded in a JEOL JEM-1400 transmission electron microscope. The sample grids for TEM have been prepared by putting one drop of the dispersion of the samples in ethyl alcohol on an amorphous carbon coated copper grid of 400 mesh. Solid state ^{13}C CP and ^{29}Si MAS NMR spectra have been recorded in a CHEMAGNETICS 300 MHz CMX 300 spectrometer. A Kratos Axis Ultra DLD system was used to collect X-ray photoelectron spectra (XPS) using monochromatic Al $K\alpha$ X-ray source operating at 120 W (10 mA x 12 kV). Data has been collected with pass energies of 160 eV for survey spectra and 20 eV for the high-resolution scans with step sizes of 1 eV and 0.1 eV, respectively. The system has been operated in the Hybrid mode, using a combination of magnetic and electrostatic lenses and acquired over an area of approximately 300 × 700 μm^2. A magnetically confined charge compensation system has been used to minimize charging of the sample surface, and all spectra have been taken with a 90° take of angle. A base pressure of *ca*. 1×10^{-9} Torr was maintained during collection of the spectra. Data was analysed using CasaXPS (v2.3.23) after subtraction of a Shirley background and using modified Wagner sensitivity factors as supplied by the manufacturer. Atomic absorption spectrophotometric (AAS) studies have been carried out in PinAAcle 900F, Perkin Elmer atomic adsorption spectrometer. For preparing sample solution, 0.04 g of **nCuO-FMS** has been dispersed in 2 ml of DTPA (diethylenetriaminepentaacetic acid) solution and the volume was made up to 20 ml by addition of distilled water. Then the solution has been shaken for 2 hours and filtered to obtain a colorless filtrate. This filtrate has been used for the analysis. ^1H NMR spectra have been collected in $CDCl_3$ solvent using a 400 MHz Bruker spectrometer with tetramethylsilane (δ = 0) as internal standard. The chemical shifts have been expressed in parts per million (δ). Mass spectra have been obtained using a Thermo ISQ QD EI Gas Chromatograph-Mass Spectrometer (GC-MS) System.

Synthesis of nCuO-FMS

Mesoporous silica, SBA-15, has been used as the solid support for the preparation of the **nCuO-FMS** catalyst. For synthesis of SBA-15,[45] 1.7 g of Pluronic P123 (poly(ethylene glycol)-blockpoly(propylene glycol)-block-poly(ethylene glycol) block copolymer) was taken in a polypropylene bottle and 62 ml of water was added to it. The mixture was vigorously stirred until all the P123 dissolved and a clear solution was obtained. Then 6 g of 35% HCl solution was added to the mixture and kept again under stirring for 15 min. Finally, 3.5 g of tetraethyl orthosilane was added drop wise to the resulting clear solution and the

reaction mixture was stirred for another 20 h at 313 K. The resulting white gel was heated at 373 K for 20 h without stirring in the polypropylene bottle under air-tight condition. Then the white mixture was cooled to room temperature, filtered and washed with water several times followed by 2-3 washings with ethyl alcohol. The white product was dried under vacuum and then calcined at 773 K for 10 hours in a flow of air to obtain the mesoporous SBA-15.

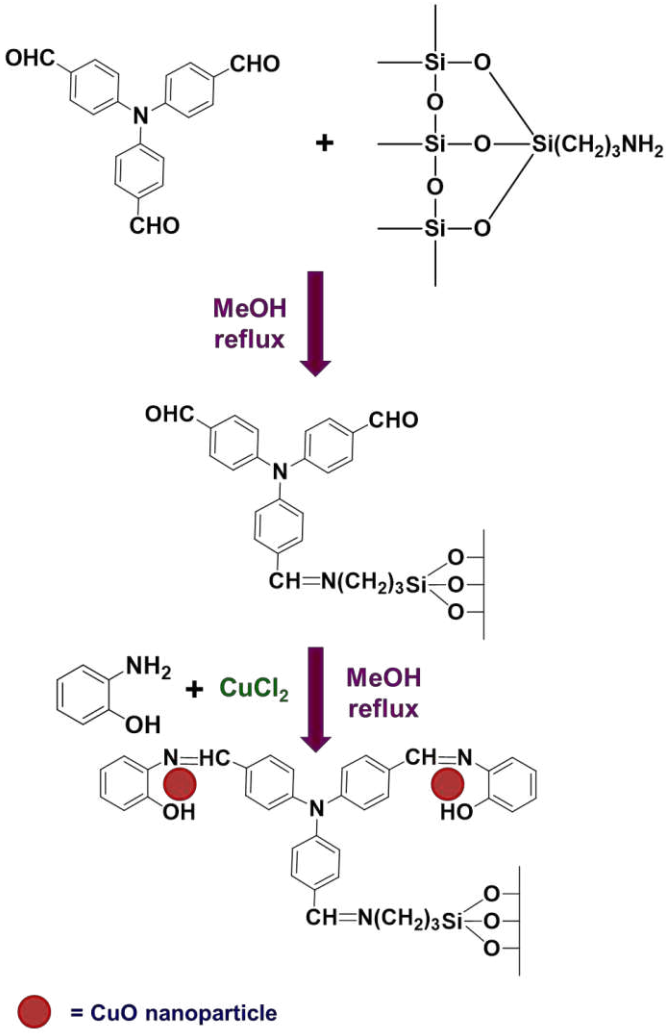

Scheme 1 Synthesis of **nCuO-FMS**

In the next step, 3-aminopropyl units were grafted on the surface of SBA-15 by stirring 1.0 g of the mesoporous silica with 1.5 g of 3-aminopropyl triethoxy silane (3-APTES) overnight in chloroform at room temperature under N_2 atmosphere. The mixture was then filtered and the product was washed repeatedly with chloroform and then dichloromethane. Finally, the $–NH_2$ functionalized SBA-15 was obtained after drying the product in vacuum. Further modification of the amine functionalized silica was carried out with

tris(4-formyl phenyl)amine, a trialdehyde (Scheme 1), which was prepared through Vilsmeier-Haack formylation reaction of triphenylamine and phosphorus oxychloride following reported procedure.[46] In this step, the trialdehyde and the $–NH_2$ functionalized SBA-15 were refluxed for 4 h in methanol and the molar ratio was kept 1:1, so that two –CHO groups of the trialdehyde remain free for further functionalization.[47] The light yellow coloured product that resulted was filtered and washed repeatedly with methanol until the filtrate became colourless.

For synthesizing **nCuO-FMS**, the *tris*(4-formyl phenyl)amine functionalized SBA-15, 2-aminophenol and $CuCl_2$ were taken in methanol in a round bottom flask. The molar ratio of the reactants was maintained at 1:2:2. Then the reaction mixture was refluxed for 4 h when the colour of the solution gradually darkened due to *in situ* formation of CuO nanoparticles. The solid product was then isolated through filtration, washed repeatedly with methanol to remove any excess reactants. Finally, the brown coloured CuO nanoparticles immobilized functionalized mesoporous silica (**nCuO-FMS**) was obtained after drying the product under vacuum.

Catalysis

In a typical catalytic reaction batch, 0.5 mmol of iodobenzene, 1 mmol Se^0 powder and 1 mmol of KOH were taken together in a round bottom flask in presence of 2.0 ml of DMSO as solvent at 363 K and under nitrogen atmosphere. The reaction was initiated with the addition of 20 mg of **nCuO-FMS** as the catalyst into it. The reaction was allowed to continue for the desired time and the solid catalyst was separated from the reaction mixture by centrifugation and washed repeatedly to remove the organic product from it. Then the product was extracted in ethyl acetate, washed thoroughly with brine solution and water for complete removal of the inorganic part. The solid product was isolated through evaporation of the solvent and purified by column chromatography in petroleum ether/ethyl acetate mixture. The isolated yield of the final product in pure form was obtained after solvent evaporation. The structure of the product isolated was characterized by ^1H NMR spectroscopy in $CDCl_3$ solvent. In addition to this, GC and GC-MS studies were used to identify the product, determine the percentage conversion and turnover frequency and number. To examine the recyclability of the catalyst, it was separated out from the reaction mixture after completion of the reaction by centrifugation. The recovered catalyst was washed repeatedly with ethyl acetate, dried and used again for another catalytic cycle of Se-Se coupling.

Results and discussion

FT-IR spectra and thermal studies

The FT-IR spectra of SBA-15, 3-APTES functionalized SBA-15, trialdehyde loaded SBA-15 and **nCuO-FMS** are recorded by ATR technique with the powdered samples and the results are shown in Fig. 1. The spectra of 3-APTES functionalized SBA-15 (Fig. 1(A)b) shows a broad band in the region of 3747-2929 cm^{-1} which may appear due to the presence of amine group and methylene moieties of the aminopropyl group.[48] For the trialdehyde loaded SBA-15 (Fig. 1(A)c) two additional peaks arise at 1643 cm^{-1} and 1698 cm^{-1}, which indicate the formation of azomethine bond and the presence of free aldehyde groups, respectively, in the material.[49] For **nCuO-FMS** (Fig. 1(A)d), the peak at 1698 cm^{-1} disappears indicating complete conversion of free –CHO groups to C=N. The band at 1647 cm^{-1} indicates the retention of azomethine moiety. The peak at *ca.* 1595 cm^{-1} may be due to the presence of aromatic C=C units which are present both in trialdehyde loaded SBA-15 and **nCuO-FMS**. For clarity, the region of interest for trialdehyde loaded SBA-15 and **nCuO-FMS** has been given in Fig. 1(B).

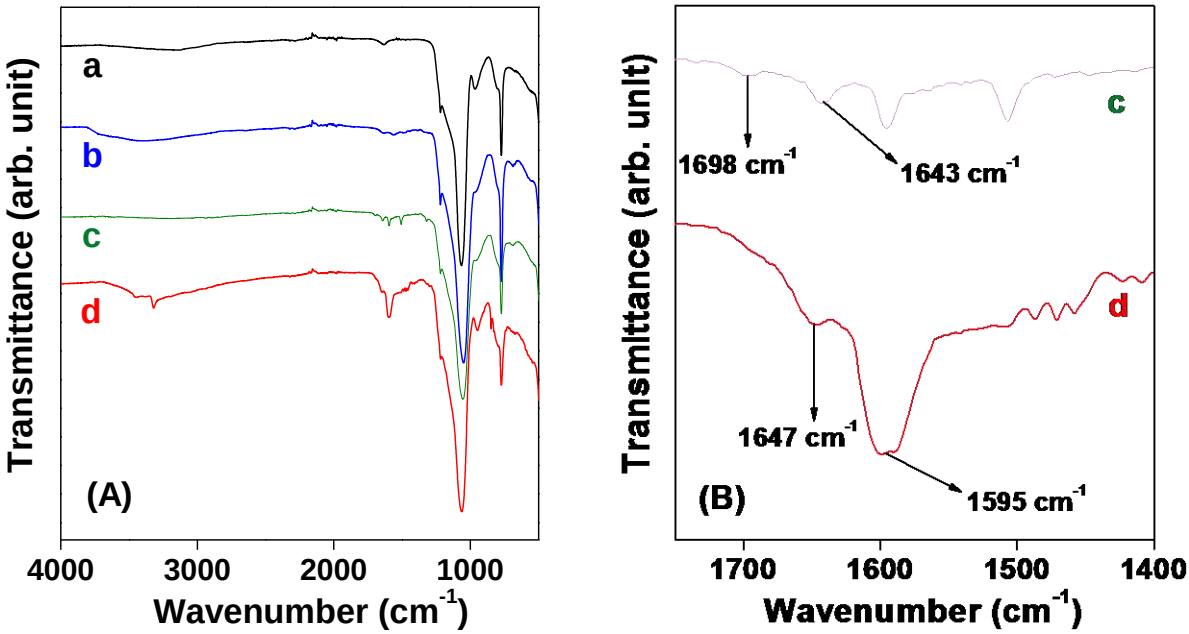

Fig. 1 (A) FT-IR spectra of (a) SBA-15, (b) 3-APTES functionalized SBA-15, (c) trialdehyde loaded SBA-15 and (d) **nCuO-FMS**; **(B)** Magnified region of plot c and d.

Thermogravimetric analyses have been carried out with the powder samples of SBA-15, 3-APTES functionalized SBA-15, trialdehyde loaded SBA-15 and **nCuO-FMS** in the temperature range of 303-1073 K to examine thermal stability of the frameworks (Fig. 2). The high thermal stability of the silica support, SBA-15 (Fig. 2a) is quite clear from the curve, where only 4% weight loss takes place up to 1073 K, mostly

due to loss of adsorbed solvent and other molecules. Such high stability makes SBA-15 a potential candidate to act as the catalyst support. The thermal stabilities of the other samples can be ascertained from their corresponding TGA plots.[50,51] All the organically modified materials (Fig. 2b-d) show stepwise weight loss corresponding to the nature and amount of the functional groups present and the mass loss continues to take place at 1073 K. For all the samples the first step of weight loss of *ca.* 3-4 % takes place at around 373 K which can be assigned to the physisorbed water molecules. For the 3-APTES functionalized SBA-15 (Fig. 2a), there is another step of weight-loss corresponding to the removal of 3-aminopropyl moieties in the sample, between the temperature range of 530 to 820 K. The TGA profile of the trialdehyde loaded SBA-15 (Fig. 2c) also shows similar trend, but the weight-loss is higher in this case due to removal of 3-aminopropyl as well as the trialdehyde units. The catalyst, **nCuO-FMS** (Fig. 2d), loses more weight in this temperature region due to removal of the 2-aminophenol units, in addition to the other organic functionalities, which plays an important role in stabilization of the CuO nanoparticles. It can also be seen from the plot that the material loses only *ca.* 5.5% of its weight up to 413 K and thus can be considered to be stable at least up to this temperature for its use as a catalyst. The percentage of functionalization in each step can be calculated from the data. The studies also give the amount of organic loading on the silica framework for each material. It can be calculated that 0.76 milimole of 3-APTES has been loaded on 1.0 g of SBA-15 and the amount of trialdehyde and 2-aminophenol is 0.18 milimole/g and 0.345 milimole/g, respectively.

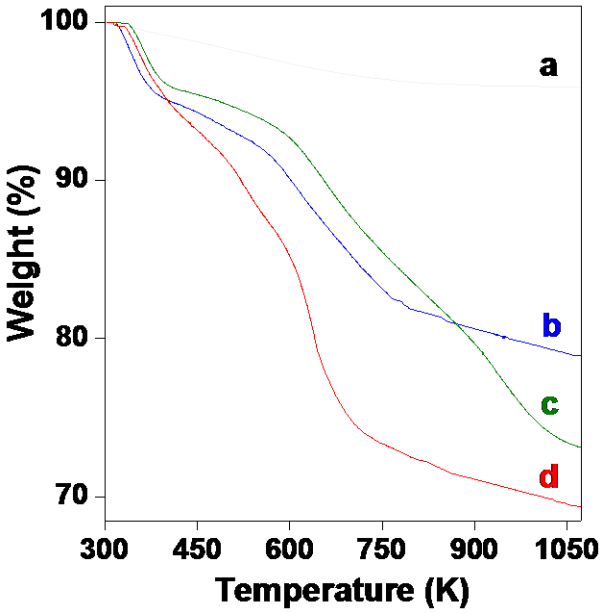

Fig. 2 Thermogravimetric study of (a) SBA-15, (b) 3-APTES functionalized SBA-15, (c) trialdehyde loaded SBA-15 and (d) **nCuO-FMS**.

Mesoporosity and microstructure

The powder X-ray diffraction patterns SBA-15, 3-APTES functionalized SBA-15, trialdehyde loaded SBA-15 and **nCuO-FMS** are given in Fig. 3. All the samples are found to show 2D-ordered hexagonal mesostructure which is evident from the presence of three distinct diffraction peaks assigned to (100), (110) and (200) planes along with a very weak one for (210) plane.[52,53] However, the intensities of the peaks get lowered and the ordering of pores are affected in the materials with gradual functionalization. In addition to this, reduction of pore size takes place which is indicated by shift of the peaks to higher 2θ values. The wide angle diffraction pattern of **nCuO-FMS** has been shown in Fig. 4. Several diffraction peaks can be observed which has been indexed in the figure and correspond to the characteristic planes of CuO.[54] Thus, it is conclusive from the figure that CuO nanoparticles have been formed in the material.

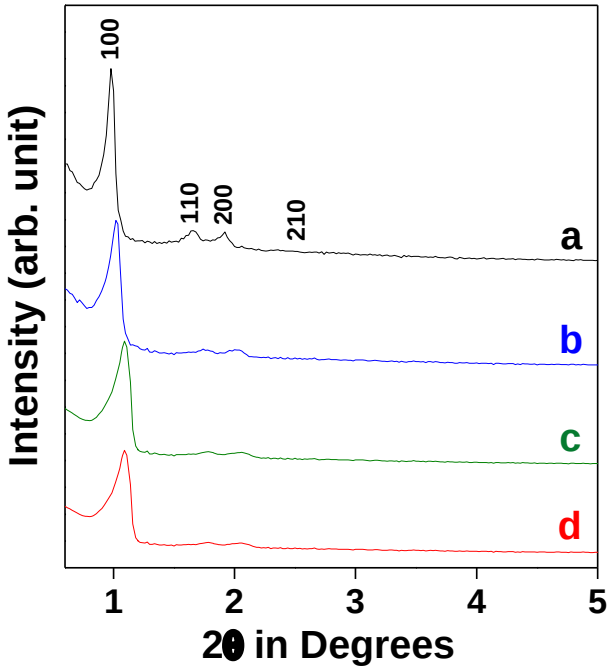

Fig. 3 Powder X-ray diffraction patterns of (a) SBA-15, (b) 3-APTES functionalized SBA-15, (c) trialdehyde loaded SBA-15 and (d) **nCuO-FMS**.

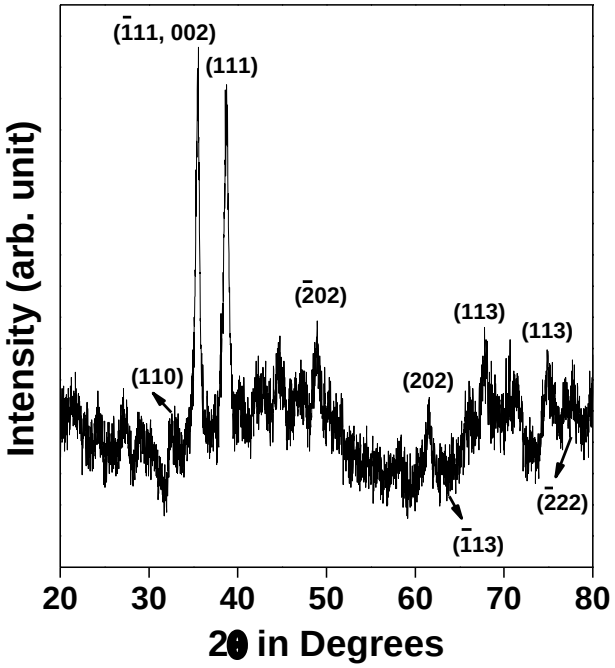

Fig. 4 Wide angle powder X-ray diffraction pattern of **nCuO-FMS**.

Nitrogen physisorption analysis can be used to determine the total surface area, pore size and pore volume of nanoporous materials. Nitrogen adsorption/desorption isotherms have been measured at 77 K for SBA-15 and all the other samples obtained after each step of functionalization. From the isotherms shown in Fig. 5, it is possible to establish the mesoporous structures of SBA-15, 3-APTES functionalized SBA-15, trialdehyde loaded SBA-15 and **nCuO-FMS**. The BET surface area, pore volume and pore size of all the samples have been presented in Table 1. Comparing these data, we can conclude that a gradual decrease in BET surface area takes place with gradual functionalization over the mesoporous SBA-15 support. This is expected as the surfaces become occupied by various organic and inorganic moieties with every step of functionalization. The pattern of the isotherms for all the samples is type IV with a steep increase in the higher pressure region because of capillary condensation. This is a characteristic of the mesoporous nature of the materials.[52,55] The isotherms of all the samples exhibit H1 type hysteresis loops between the P/P_0 values of 0.6 and 1.0 which is attributed to the presence of well-defined cylindrical pore channels[56] as well as intercrystallite adsorption.[57] The average pore diameter of the starting mesoporous SBA-15 from the NLDFT model is 7.86 nm (Inset of Fig. 5). Pore sizes of the functionalized materials follow a gradual descending trend as incorporation of functional groups on the pore walls of the silica support inhibits access of nitrogen gas molecules into the pores. Similar decreasing trend is also observed for the pore volume of the samples.

Table 1 Surface area, pore volume and pore size of the samples at various stages

	Sample	BET surface area (m^2/g)	Pore volume (cc/g)	Pore size (nm)
(a)	SBA-15	732	0.966	8.15
(b)	3-APTES functionalized SBA-15	366	0.652	7.45
(c)	Trialdehyde loaded SBA-15	243	0.315	5.95
(d)	**nCuO-FMS**	133	0.205	4.75

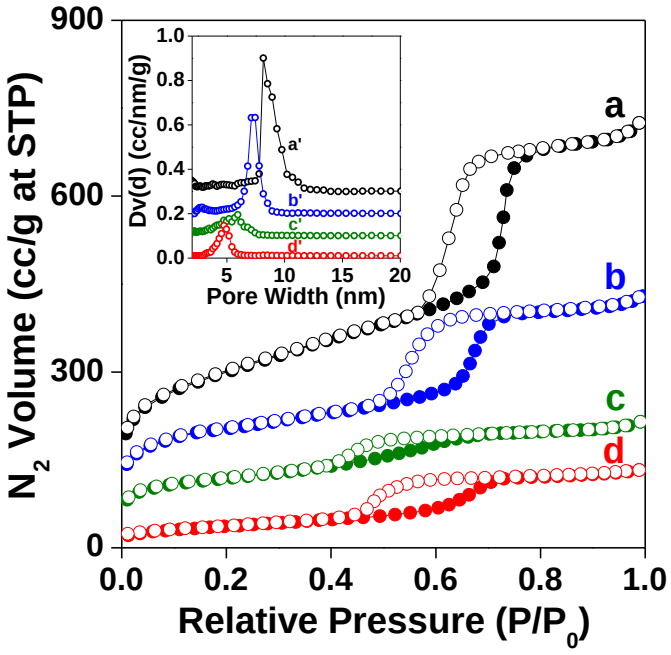

Fig. 5 Nitrogen adsorption desorption isotherms of (a) SBA-15, (b) 3-APTES functionalized SBA-15, (c) trialdehyde loaded SBA-15 and (d) **nCuO-FMS**. For clarity, the Y-axis values have been increased by 100, 100 and 50 cc/g for plot a, b and c, respectively. Adsorption points are marked by filled symbols and desorption points by empty symbols.

Inset: NLDFT Pore size Distribution of (a') SBA-15, (b') 3-APTES functionalized SBA-15, (c') trialdehyde loaded SBA-15 and (d') **nCuO-FMS**. Y-axis values have been increased by 0.3, 0.25 and 0.15 cc/nm/g, for plot a', b' and c', respectively.

The transmission electron microscopic (TEM) images of SBA-15, trialdehyde loaded SBA-15 and **nCuO-FMS** are shown in Fig. 6. The image for SBA-15 (Fig. 6a) confirms the formation of a well-formed hexagonally arranged mesoporous structure as desirable for an appropriate solid support. Upon functionalization the long range ordering of the pores is decreased to some extent, however, the basic

hexagonal structure is retained quite well. The TEM image of **nCuO-FMS** is shown in Fig. 6c. Spherical CuO particles with diameter *ca.* 6-7 nm could be seen dispersed throughout the matrix of the mesoporous silica confirming the *in situ* generation of the nanoparticles. Thus, powder X-ray diffraction, N_2 sorption experiments and TEM image analyses of the samples establish their microstructure and mesoporosity. In addition to that, the formation of CuO nanoparticles over the functionalized silica support can also be established from the studies. The amount of Cu^{2+} present in **nCuO-FMS** has been ascertained from atomic absorption spectrophotometric study. It has been found that 1.0 g of **nCuO-FMS** contains 2.096×10^{-4} mole or 13.32 mg of Cu^{2+}.

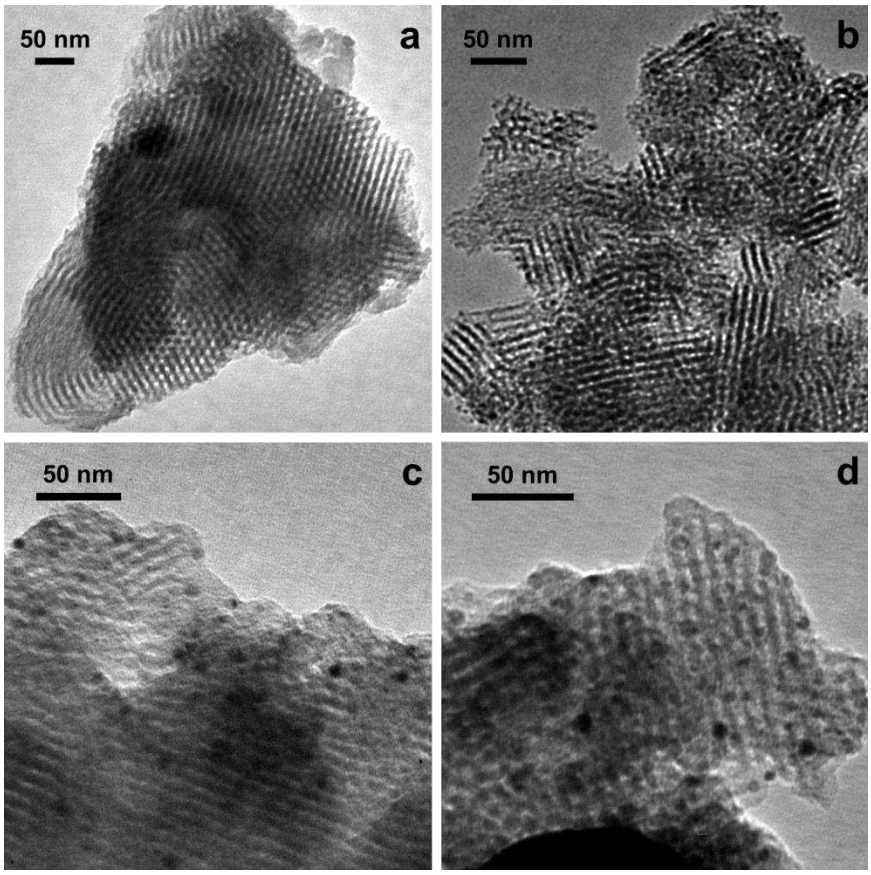

Fig. 6 TEM images of (a) SBA-15, (b) trialdehyde loaded SBA-15 and (c) **nCuO-FMS** and (d) reused **nCuO-FMS**.

Solid state NMR studies

The chemical environments around the silicon atom in the synthesized materials have been studied by ^{29}Si MAS NMR and the results are given in Fig. 7. For SBA-15, peaks are obtained at *ca*. –111.65 and

–103.17 ppm (Fig. 7a) which can be assigned to the Q^4 and Q^3 silica centers of the $Si(OSi)_n(OH)_{4-n}$ units. For the 3-APTES functionalized SBA-15 (Fig. 7b), apart from peaks for Q_4 and Q_3 silica species, additional peaks appear at –67.0 and –58.06 ppm due to incorporation of the aminopropyl group in the matrix. The chemical environment of the starting silica support changes due to such addition of aminopropyl groups and the new peaks can be attributed to the T^3 ($(SiO)_3Si$-R-$Si(OSi)_3$) and T^2 ($(HO)_2(OSi)Si$-R-$Si(OSi)_2(OH)$) species,[58,59] respectively. The spectra for other two samples, trialdehyde loaded SBA-15 and **nCuO-FMS** (Fig. 7c and d, respectively), show similar pattern as the 3-APTES modified SBA-15 which indicates formation and retention of imine bonds in both the samples. A marginal shifting of peak position is observed for **nCuO-FMS** (Fig. 7d) due to formation of CuO nanoparticles which are stabilized by N and O groups of the functionalized silica framework through non-covalent interactions.[60,61]

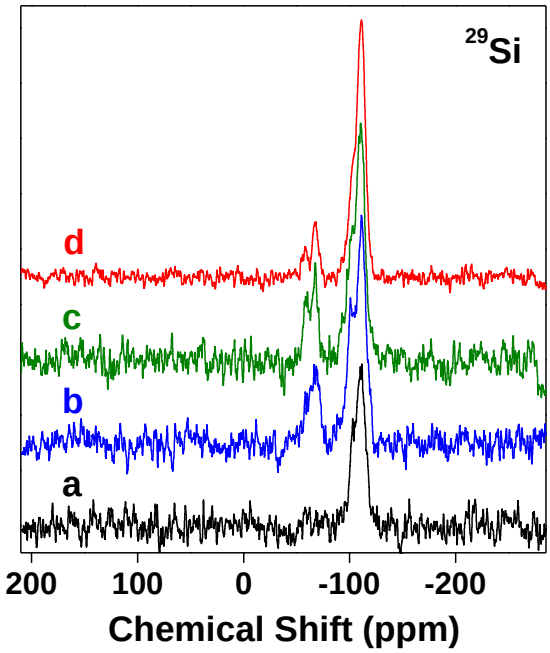

Fig. 7 Solid state ^{29}Si MAS NMR spectra of (a) SBA-15, (b) 3-APTES functionalized SBA-15, (c) trialdehyde loaded SBA-15 and (d) **nCuO-FMS**.

^{13}C CP MAS NMR studies have been performed with the materials having organic contents and the spectra are shown in Fig.8. Spectrum for 3-APTES functionalized SBA-15 (Fig. 8a) shows peaks at 9.71, 22.39, 29.17 and 42.86 ppm. The signal at 42.86 ppm may be attributed to the carbon adjacent to the amine group, the signals at 29.17 and 22.39 ppm may appear due to the α and β carbon atoms with respect to the $–NH_2$ group and the signal at 9.71 ppm for other aliphatic carbon atoms. For the trialdehyde loaded SBA-15 (Fig. 8b) several new peaks emerge at 10.47, 21.84, 42.86 and 63.98 ppm for the aliphatic carbon

atoms and at 151, 164.84 and 128.95 ppm for the aromatic carbon atoms. Two characteristics peaks at183.72 and 199.78 ppm appear due to the formation of C=N bond (imine bond) and the free aldehyde group, respectively. From this spectrum we can conclude that Schiff base reaction has taken place between the trialdehyde and 3-APTES loaded silica and at the same time residual free aldehyde groups are also present. For **nCuO-FMS** (Fig 8c), the peaks corresponding to aliphatic and aromatic regions are found to remain almost intact. However, two new peaks appear at 147.76 and 163.67 ppm which may be attributed to the aromatic carbon attached to the phenolic –OH group and imine bond formation, respectively. The peak at 163.67 ppm confirms complete conversion of the residual –CHO groups of trialdehyde to C=N after condensation with 2-aminophenol.

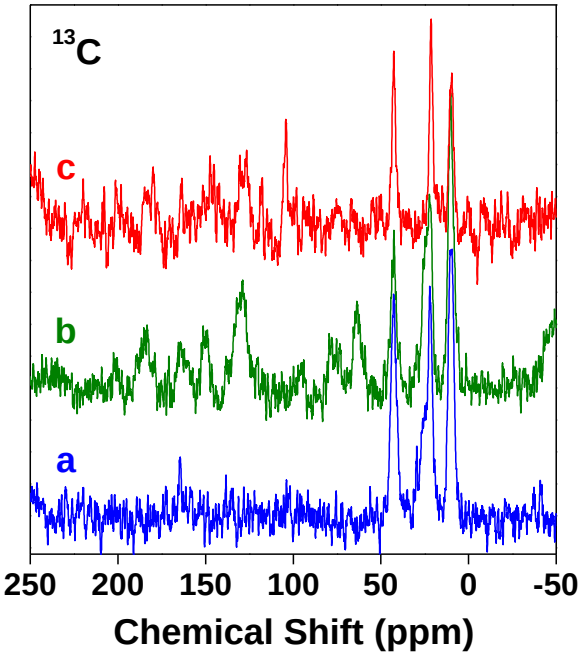

Fig. 8 Solid state ^{13}C CP-MAS NMR spectra of (a) 3-APTES functionalized SBA-15, (b) trialdehyde loaded SBA-15 and (c) **nCuO-FMS**.

XPS analysis

The wide scan and fitted XPS spectra of **nCuO-FMS** has been shown in Fig. 9. The survey spectrum (Fig. 9a) reveals the presence of Si, C, O, N and Cu in the material, in agreement with the expected elemental distribution. The Cu(2p) spectra (Fig. 9b), reveals two states with binding energies of 934.6 eV and 932.1 eV and assigned to the Cu $2p_{3/2}$ states, for Cu(II), in CuO and reduced Cu respectively; the lower binding energy species, we attribute to the reduction of the Cu(II) species during analysis.[62,63] Fig. 9c and 9d show the multiple states of oxygen and carbon present within the material. The peak at 532.7 eV is assigned primarily to Si-O

bonds, although the presence of carbon-oxygen functions at this energy also cannot be discounted. The peaks at 531.1 and 533.8 eV can be ascribed to inorganic (Cu-O)[64] and organic oxygen, respectively. The binding energies of different types of carbon present in the sample have been illustrated in Fig. 9d. Four distinct peaks appear at 284.3, 284.7, 286 and 287.1 eV and assigned to the presence of C=C, C-C, C-O and C=O species in **nCuO-FMS**, respectively.[65]

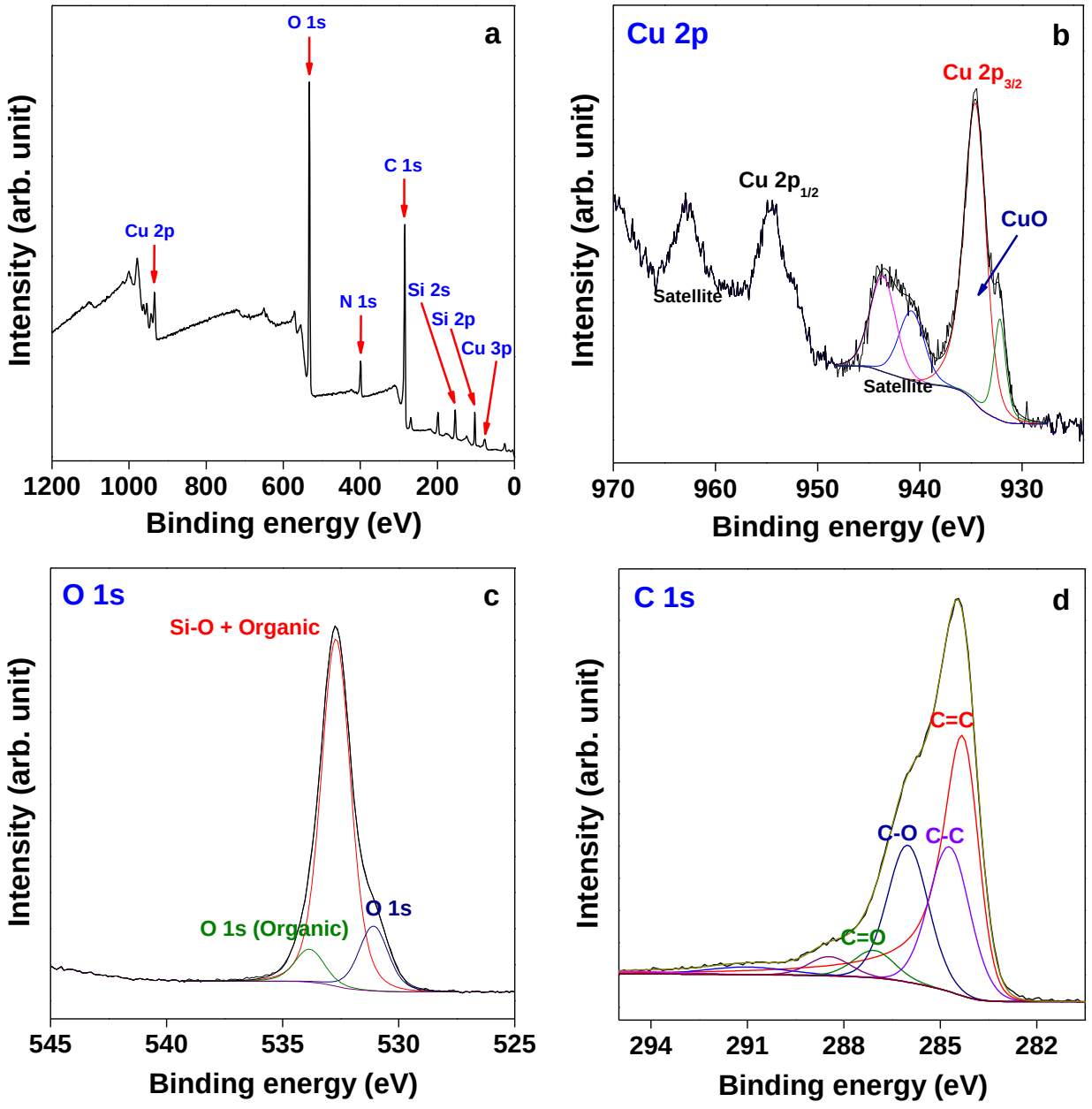

Fig. 9 XPS spectra of **nCuO-FMS** (a) wide scan, (b) Cu 2p core-level, (c) O 1s core-level and (d) C 1s core-level.

Catalytic studies

The catalytic efficiency of **nCuO-FMS** has been studied for Se-Se coupling reaction under different reaction conditions (Table 2). To begin with, different amounts of **nCuO-FMS** are used to study the reaction between iodobenzene (0.5 mmol), Se^0 powder (1.0 mmol) and KOH (1.0 mmol) in 2.0 ml dimethyl sulphoxide (DMSO) at 363 K under nitrogen atmosphere to find out the maximum yield. The product obtained is 1,2-diphenyl diselenide (**3a**). The reaction did not produce significant amount of the product when 1 mg of **nCuO-FMS** is used for the catalytic reaction (entry 1). With gradual increase in the amount of the catalyst to 2, 5 and 10 mg (entries 2-4), the yield was found to increase slowly to 25, 46 and 64%, respectively. When the amount of **nCuO-FMS** is increased to 20 mg the yield reached to 78% (entry 5) and this is the maximum value at the given temperature. When the amount of catalyst is increased further to 30 mg the product formation is not affected much and the yield is 79% (entry 6). Thus, it can be established that 20 mg of **nCuO-FMS** is sufficient for achieving the best yield of **3a** for this optimization reaction under the specified conditions. After this, the base is altered; KOH is replaced by NaOH and the yield is found to be lower at 67% (entry 7). Then the reaction is carried out by changing the solvent to dimethyl formamide (DMF) and acetonitrile (CH_3CN), and the yields reduce to 73 and 63% (entries 8 and 9), respectively. Finally, the reaction is performed at different temperatures. Increasing the temperature to 373 K did not improve the amount of product formed (78% yield, entry 10) while by decreasing the temperature to 333 K a lower yield (55%, entry 11) is obtained.

Table 2 Optimization of the catalytic conditions[a]

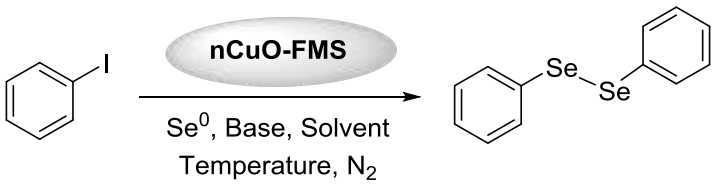

Entry	**nCuO-FMS** (in mg)	Base	Temperature (K)	Solvent	Isolated Yield (%)[b]	TON	TOF
1	1	KOH	363	DMSO	trace	-	-
2	2	KOH	363	DMSO	25	29.82	9.940
3	5	KOH	363	DMSO	46	54.87	18.288
4	10	KOH	363	DMSO	64	76.35	25.445
5	20	KOH	363	DMSO	78	93.03	31.011
6	30	KOH	363	DMSO	79	94.23	31.409
7	20	NaOH	363	DMSO	67	79.91	26.638
8	20	KOH	363	DMF	73	87.07	29.023
9	20	KOH	363	CH_3CN	63	75.14	25.05
10	20	KOH	373	DMSO	78	93.03	31.011
11	20	KOH	333	DMSO	55	65.60	21.867

[a]All the reactions are carried out for 3 h with 0.5 mmol of substrate, 1.0 mmol Se^0 and 1.0 mmol of base.
[b]Yields determined by NMR spectroscopy

To study the time dependent conversion of iodobenzene to 1,2-diphenyl diselenide, the reaction in DMSO solvent is then carried out for different time periods (Table 3). It can be seen that the conversion increases marginally as the reaction time is increased from 3 h to 6, 9 and 12 h. After 12 h the isolated yield obtained is 83% (entry 4) which is little better than the 78% yield that is obtained within 3 h (entry 1) of the reaction. So, it can be concluded that if the reaction time is increased the yields do not increase significantly, and thus in the present study the reaction time has been optimized at 3 h. However, it should be noted that isolated yields are always lower than the actual conversion in a reaction since some amount of the product is lost during the process of work-up, isolation and purification and of the final reaction mixture.

Table 3 Time dependent conversion of iodobenzene in catalytic Se-Se coupling reaction[a]

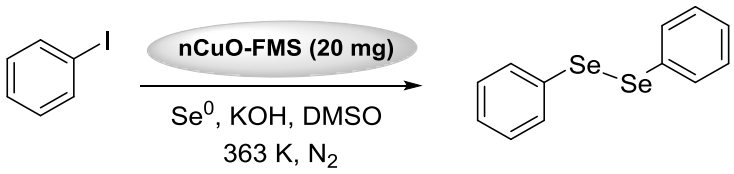

Entry	Time (h)	Isolated Yield (%)[b]	TON	TOF
1	3	78	93.03	31.01
2	6	80	95.42	31.81
3	9	81	96.61	32.20
4	12	83	99.00	33.00

[a]The reaction has been are carried out in 10 ml of acetonitrile as solvent with 2.5 mmol of iodobenzene, 5.0 mmol of Se^0 powder and 5.0 mmol of KOH, at 363 K using 0.1 g of **nCuO-FMS** as catalyst. [b]Yields determined by NMR spectroscopy

After determining the optimized reaction condition, the conversions have been carried out using various substituted iodobenzenes to produce the corresponding 1,2-diphenyl diselenide derivatives (Table 4). When 4-methyl iodobenzene and 3-methyl iodobenzene are used the products, 1,2-di-*p*-tolyldiselane (**3b**) and 1,2-di-*m*-tolyldiselane (**3c**), are obtained with very good yields of 77 and 75%, respectively. To explore the scope of substrate for the reactions, substituted iodobenzenes with different groups (-F, -Cl, -Br, $-CF_3$) have been studied. 4-fluoro iodobenzene reacted to form 1,2-*bis*(4-fluorophenyl)diselenide (**3d**) with 74% yield, 4-chloro iodobenzene formed 1,2-*bis*(4-chlorophenyl)diselenide (**3e**) with 76% yield and 4-bromo iodobenzene formed 1,2-*bis*(4-bromophenyl)diselenide (**3f**) with 75% yield. 3-trifluoromethyl iodobenzene gives 1,2-*bis*(3-(trifluoromethyl)phenyl)diselenide (**3g**) as the product with 72% yield. A heterocyclic iodo compound, 2-iodothiophene, has also been used for the study. The product, 1,2-*di*(thiophen-2-yl)diselenide (**3h**), is obtained and the yield is 73%. Thus, it is observed that iodobenzene with no substituent gives the finest result among the substrates.

Table 4 Catalytic Se-Se coupling reactions using different substrates[a]

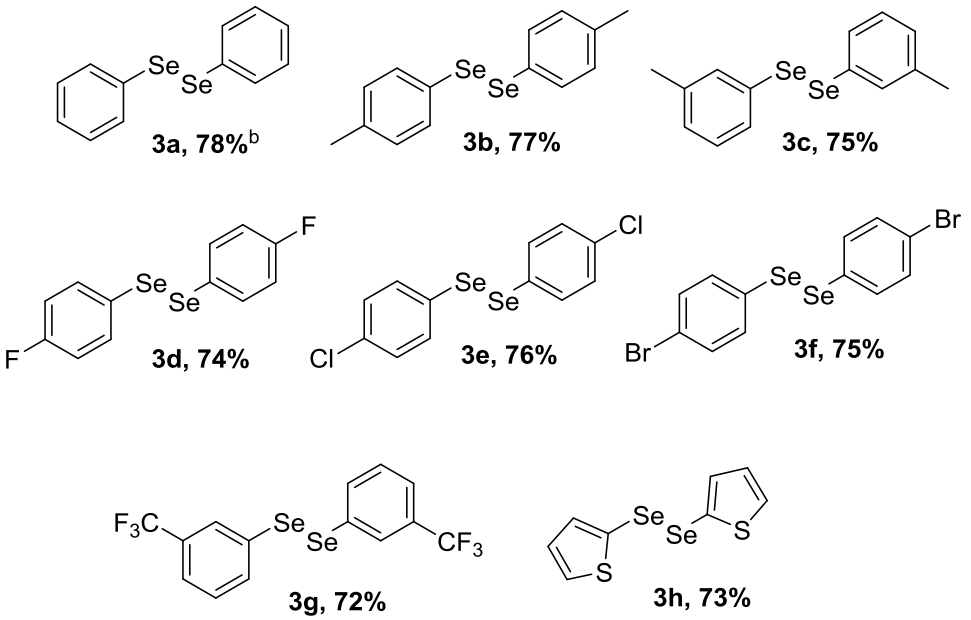

Entry	R/Substrate	Isolated Yield (%)[b]	TON	TOF
3a	--	78	93.03	31.01
3b	4-CH_3	77	91.84	30.61
3c	3-CH_3	75	89.46	29.82
3d	4-F	74	88.26	29.42
3e	4-Cl	76	90.65	30.22
3f	4-Br	75	89.46	29.82
3g	3-CF_3	72	85.88	28.63
3h	2-iodothiophene	73	87.07	29.02

[a]The reactions have been carried out for 3 h in 2 ml of DMSO as solvent with 0.5 mmol of the respective substrates, 1.0 mmol of Se^0 powder and 1.0 mmol of KOH, at 363 K using 20 mg of **nCuO-FMS** as catalyst.
[b]Yields determined by NMR spectroscopy

The ^1H NMR, ^{13}C NMR, ^{77}Se NMR and mass spectra are given in supplementary information with the structure of the corresponding compounds.

Recyclability

The ability to recycle is the most attractive feature of a heterogeneous catalyst. In this work, to study the recyclability of **nCuO-FMS** in Se-Se coupling the reaction iodobenzene as the substrate has been studied under the optimized condition. In each cycle, 0.5 mmol of iodobenzene, 1.0 mmol of Se^0 powder and 1.0 mmol of KOH are taken in 2.0 ml of DMSO and the reaction is carried out at 363 K under nitrogen atmosphere for 3 h. Then the catalyst is recovered, regenerated and reused in the subsequent run. The conversion (%) against the number of reaction cycles for the coupling has been given in Fig. 10. The percentage conversions in five cycles are 78, 78, 75, 70 and 68%, respectively. It can be seen that the efficiency of the catalyst remains more or less same in the first two cycles. After that there is marginal drop in the percentage of conversion in each step and after five cycles it is 68%. The gradual drop of conversion from the first to the fifth cycle may be attributed to partial damage of the mesoporous structure of the catalyst when it remains in the matrix of the catalytic system for prolong period during the reactions. Thus, it can be inferred that the catalyst has good recycling efficiency. The TEM image of recycled **nCuO-FMS** is illustrated in Fig. 6d. It shows that the porous structure of the mesoporous silica matrix is retained even after the catalytic performance and the immobilization of the CuO nanoparticles over it also remains intact. In addition to this, the surface area of the recycled catalyst is also not reduced to a large extent which adds to the reusability of the material as catalyst.

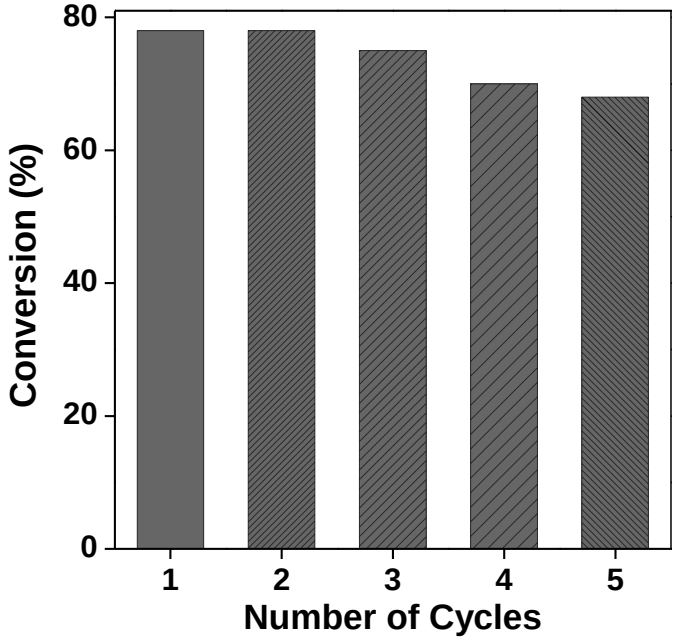

Fig. 10 Recycling efficiency of **nCuO-FMS** for Se-Se coupling using iodobenzene

Mechanism

A plausible mechanism[66] can be proposed for the Se-Se coupling reaction and it is shown in Scheme 2. In presence of a base, selenium gives selenide or selenite anion and in a super basic DMSO/KOH medium a reductive dimsyl species is produced. The dimsyl species is responsible for the formation of the desired diselenide anion. This preformed anion is considered to be the active species involved in the catalytic cycle. The formation of species **a** and **b** take place by the ligand exchange with the diselenide anion and may further generate complex **c**. Then, species **c** may undergo reductive elimination *via* formation of initial coupling product **d** and CuO nanoparticles in **nCuO-FMS** are regenerated. Then **d** probably reacts with another unit of **b** to form a new complex **e**. Finally, the desired diselenide compound **f** is formed by another step of reductive elimination and the other unit of CuO nanoparticles of **nCuO-FMS** could be regenerated. The CuO nanoparticles thus recovered can be used in the next catalytic cycle.

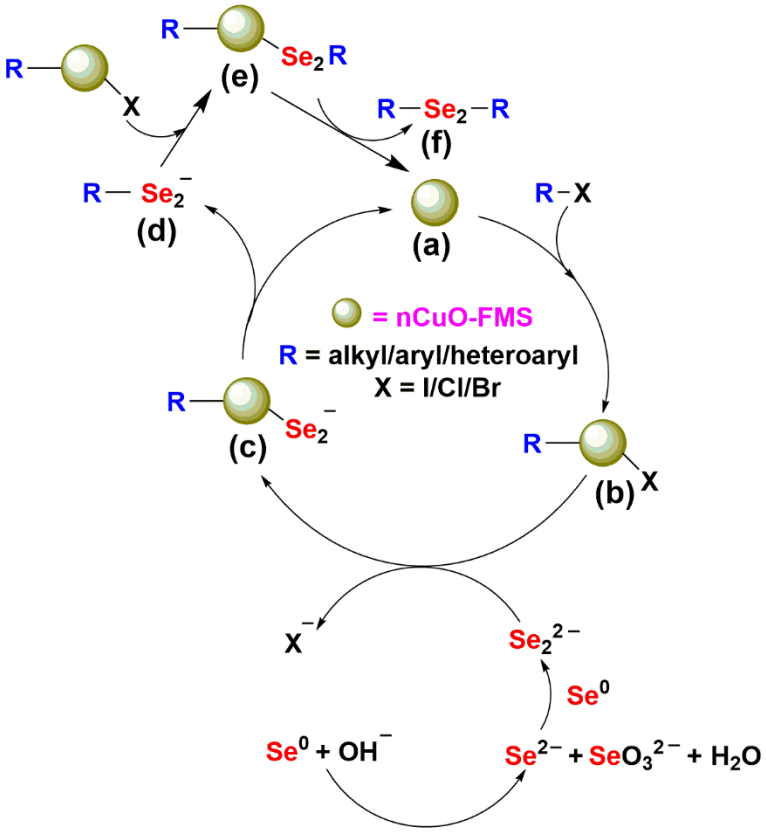

Scheme 2 Plausible mechanism for organo diselenide synthesis

Conclusions

In this article, we have synthesized a mesoporous silica based catalyst with immobilized CuO nanoparticles, **nCuO-FMS**, using a facile synthetic route. The generation of CuO nanoparticles took place *in situ* in presence of 2-aminophenol, which also acted as a stabilizing support to the metal oxide particles. The silica support, SBA-15 and all other subsequent organically functionalized frameworks, including the catalyst have been characterized thoroughly to establish their structure. This CuO nanoparticles containing porous silica with good specific surface area is found to catalyze Se-Se coupling reaction to produce symmetrical diselenides with high yields. Thus, it provides a simple and efficient method for the preparation of diselenides through cross-coupling reaction between selenium and aryl iodides. The process is chemoselective and can be used to prepare a wide range of substituted symmetrical diselenides containing *e.g.* methoxy, carboxylate, hydroxyl, amino, aldehyde and bromo groups. The superior activity of the catalyst can be attributed to the nanoscale dimension of the CuO particles as well as high surface area of the silica matrix which predisposes the substrates better at the catalytically active metal centres. The catalyst is cheaper than commercially available CuO nanopowder and due to its heterogeneous nature it can be economically used for several reaction cycles.

Acknowledgements

MN thanks DST-SERB, India (SB/FT/CS-004/2014 dated 27/06/2014) and WB-DST, India (ST/P/S&T/15G-20/2018) for financial support. Authors are thankful to N Pradhan and J Guin of Indian Association for the Cultivation of Science for providing TEM and GC-MS facilities and G Ghosh of Visva-Bharati for AAS studies.

References

1.	K.C. Gupta, A. K. Sutar and C.-C. Lin, *Coord. Chem. Rev.*, 2009, **253**, 1926.
2.	D. R. Godhani, H. D. Nakum, D. K. Parmar, J. P. Mehta and N. C. Desai, *J. Mol. Catal. A*, 2017, **426**, 223.
3.	M.TruebaandS. P. Trasatti, *Eur. J. Inorg. Chem*., 2005, **17**, 3393.
4.	E. L. Margelefsky, R. K. Zeidan and M. E. Davis, *Chem. Soc. Rev.*, 2008, **37**, 1118.
5.	A. Zarnegaryan, M. Moghadam, S. Tangestaninejad, V. Mirkhani and I. Mohammdpoor-Baltork, *New J. Chem.*, 2016, **40**, 2280.
6.	Y. Zhang, A. Wang and T. Zhang, *Chem. Commun.*, 2010, **46**, 862.
7.	J. M. Planeix, N. Coustel, B. Coq, V. Brotons, P. S. Kumbhar, R. Dutartre, P. Geneste, P. Bernier and P. M. Ajayan, *J. Am. Chem. Soc.*, 1994, **116**, 7935.
8.	A. Dhakshinamoorthy and H. Garcia, *Chem. Soc. Rev.*, 2014, **43**, 5750.
9.	S. Zhou, M. Johnson and J. G. C. Veinot, *Chem. Commun.*, 2010, **46**, 2411.
10.	H. Noh, Y. Cui, A. W. Peters, D. R. Pahls, M. A. Ortuñ, N. A. Vermeulen, C. J. Cramer, L. Gagliardi, J. T. Hupp and O. K. Farha, *J. Am. Chem. Soc.*, 2016, **138**, 14720.
11.	C. M. A. Parlett, K. Wilson and A. F. Lee, *Chem. Soc. Rev.*, 2013, **42**, 3876.
12.	T. Toyao, K. Miyahara, M. Fujiwaki, T.-H. Kim, S. Dohshi, Y. Horiuchi and M. Matsuoka, *J. Phys. Chem. C*, 2015, **119**, 8131.
13.	R. M. Rioux, H. Song, J. D. Hoefelmeyer, P. Yang and G. A. Somorjai, *J. Phys. Chem. B*, 2005, **109**, 2192.
14.	C. Xu, X. Wang, J. Zhu, X. Yang and L. Lu, *J. Mater. Chem.*, 2008, **18**, 5625.
15.	G.B. Shul'pin, *Catalysts*, 2016, **6**, 50.
16.	K.C. Gupta and A. Kumar Sutar, *Coord. Chem. Rev*., 2008, **252**, 1420.
17.	M. B.Thathagar, J. Beckers andG. Rothenberg,*J. Am.Chem. Soc*., 2002, **124**, 11858.
18.	T. Kamal, *Polymer Testing*, 2019, **77**, 105896.
19.	L. Xu, J. Zhang, Z. Li, Q. Ma, Y. Wang, F. Cui and T. Cui, *New J. Chem.*, 2019, **43**, 520.
20.	X. Xiong, C. You, Z. Liu, A. M. Asiri, X. Sun, *ACS Sustainable Chem. Eng.*, 2018, **6**, 2883.
21.	S. Vásquez-Céspedes, K. M. Chepiga, N. Möller, A. H. Schäfer and F. Glorius, *ACS Catalysis*, 2016, **6**, 5954.
22.	N. K. Ojha, G. V. Zyryanov, A. Majee, V. N. Charushin, O. N. Chupakhin and S. Santra, *Coord. Chem. Rev*., 2017, **353**, 1.
23.	A. Fihri, M. Bouhrara, B. Nekoueishahraki, J.-M. Basset, V. Polshettiwar, *Chem. Soc. Rev*. 2011, **40**, 5181.

24.	G. Mugesh, W.W. du Mont and H. Sies, *Chem. Rev*., 2001, **101**, 2125.
25.	C. W. Nogueira and J. B. T. Rocha, *Arch.Toxicol.*, 2011, **85**, 1313.
26.	K. Didehban, E. Vessally, A. Hosseinian, L. Edjlali and E. S. Khosroshahi, *RSC Adv*., 2018, **8**, 291.
27.	V.Nascimento, E. E. Alberto, D. W. Tondo, D. Dambrowski, M. R. Detty, F. Nome andA. L. Braga, *J. Am. Chem. Soc.*, 2012, **134**, 138.
28.	D. M. Freudendahl, S. Santoro, S. A. Shahzad, C. Santi and T. Wirth, *Angew. Chem., Int. Ed*., 2009, **48**, 8409.
29.	A. Gucchait, N. Joardar, P. K. Parida, P. Roy, N. Mukherjee, A. Dutta, R. Yesuvadian, S. P. SinhaBabu, K. Jana and A. K. Misra, *Eur. J. Med. Chem.*, 2018, **143**, 598.
30.	D. Plano, Y. Baquedano, D. Moreno-Mateos, M. Font, A. Jiménez-Ruiz, J.A. Palop and C. Sanmartín, *Eur. J. Med. Chem.*, 2011, **46**, 3315.
31.	P. G. Geiger, F. Lin and A. W. Girotti,*Free Radical Biol. Med*., 1993, **14**, 251.
32.	E.E. Alberto, V. Nascimento and A.L. Braga, *J. Braz. Chem. Soc*., 2010, **21**, 2032.
33.	C. W. Nogueira, G. Zeni andJ. B. T. Rocha, *Chem. Rev*., 2004, **104**, 6255.
34.	E.R.T. Tiekink, *Dalton Trans.*, 2012, **41**, 6390.
35.	G. I. Dzhardimalieva and I. E. Uflyand, *J. of Coord. Chem.*, 2019, **72**, 1.
36.	T. Manna, A. K. Misra, *SynOpen*, 2018, **2**, 229.
37.	D. Tanini, A. Degl'Innocenti and A. Capperucci, *Eur. J. Org. Chem*., 2015, **2**, 357.
38.	M. A. Rizvi, S. Guru, T. Naqvi, M. Kumar, N. Kumbhar, S. Akhoon, S. Banday, S. K. Singh, S. Bhushan, G. Mustafa Peerzada and B. A. Shah, *Bioorg. Med. Chem. Lett.*, 2014, **24**, 3440.
39.	Z. Li, F. Ke, H. Deng, H. Xu, H. Xiang and X. Zhou, *Org. Biomol. Chem*., 2013, **11**, 2943.
40.	G. V. Botteselle, M. Godoi, F. Z. Galetto, L. Bettanin, D. Singh, O. E. Rodrigues and A. L. Braga, *J. Mol. Catal. A: Chem*., 2012, **365**, 186.
41.	A. Krief, W. Dumont and C. Delmotte, *Angew. Chem. Int. Ed.*, 2000, **39**, 1669.
42.	F. Tian, Z. Yu and S. Lu, *J. Org. Chem.*, 2004, **69**, 4520.
43.	P. Salama and C. Bernard, *Tetrahedron Lett.*, 1998, **39**, 745.
44.	D. Singh, A.M. Deobald, L.R.S. Camargo, G. Tabarelli, O.E.D. Rodrigues and A.L. Braga, *Org. Lett.*, 2010, **12**, 3288.
45.	D. Zhao, J. Feng, Q. Huo, N.Melosh, G.H. Fredrickson, B.F.Chmelka and G.D. Stucky, *Science*, 1998, **279**, 548.
46.	T. Mallegol, S. Gmouh, M. A. A. Meziane, M. B.-Desce and O. Mongin, *Synthesis*, 2005, **11**, 1771.

47.	T. Das, H. Uyama and M. Nandi, *New J. Chem.*, 2018, **42**, 6416.
48.	D. Singha, T. Das, L. Satyanarayana, P. Roy and M. Nandi, *New J. Chem.*, 2019, **43**, 15563.
49.	K. Sarkar, K. Dhara, M. Nandi, P. Roy, A. Bhaumik and P. Banerjee, *Adv. Funct. Mater*., 2009, **19**, 223.
50.	C. Sarkar, P. Koley, I. Shown, J. Lee, Y.-F. Liao, K. An, J. Tardio, L. Nakka, K.-H. Chen and J. Mondal, *ACS Sustainable Chem. Eng.*, 2019, **7**, 10349.
51.	S. K. Verma and V. K. Singh, *J. Coord. Chem.*, 2015, **68**, 1072.
52.	A. P. Wight and M. E. Davis, *Chem. Rev*., 2002, **102**, 3589.
53.	O. Olkhovyk and M. Jaroniec, *J. Am. Chem. Soc.*, 2005, **127**, 60.
54.	V. V. T. Padil and M. Černík, *Int. J. Nanomed.*, 2013, **8**, 889.
55.	A. Stein, *Adv. Mater*., 2003, **15**, 763.
56.	M. Thommes, K. Kaneko, A. V. Neimark, J. P. Olivier, F. Rodriguez-Reinoso, J. Rouquerol, K. S. Sing,*Pure Appl. Chem.*, 2015, **87**, 1051.
57.	T. Tanev and T. J. Pinnavaia, *Science*, 1996, **271**, 1267.
58.	S. Inagaki, S. Guan, Y. Fukushima, T. Ohsuna and O. Terasaki, *J. Am. Chem. Soc.*, 1999, **121**, 9611.
59.	S. Inagaki, S. Guan, T. Ohsuna and O. Terasaki, *Nature*, 2002, **416**, 304.
60.	C. Sarkar, S. Pendem, A. Shrotri, D. Q. Dao, P. P. T. Mai, T. N. Ngoc, D. R. Chandaka, T. V. Rao, Q. T. Trinh, M. P. Sherburne and J. Mondal, *ACS Appl. Mater. Interfaces*, 2019, **11**, 11722.
61.	S. C. Shit, R. Singuru, S. Pollastri, B. Joseph, B. S. Rao, N. Lingaiah and J. Mondal, *Catal. Sci. Technol.*, 2018, **8**, 2195.
62.	L. Xu , J. Zhang , Z. Li , Q. Ma , Y. Wang, F. Cui and T. Cui, *New J. Chem.*, 2019, **43**, 520.
63.	T. L. Freeman, S. D. Evans and A. Ulman, *Thin Solid Films*, 1994, **244**, 784.
64.	H. Wang, J. -Z. Xu, J. -J. Zhu and H. -Y. Chen, *J. Cryst. Growth*, 2002, **244**, 88.
65.	Y. Liu, L. Ma, D. Zhang, G. Han and Y. Chang, *RSC Adv*., 2017, **7**, 12027.
66.	V. P. Reddy, A. V. Kumar, K. Swapna and K. R. Rao, *Org. Lett.*, 2009, **11**, 951.